

A fast and scalable computational framework for goal-oriented linear Bayesian optimal experimental design: Application to optimal sensor placement

Keyi Wu¹, Peng Chen², and Omar Ghattas²

¹Department of Mathematics, University of Texas at Austin, Austin, USA

²Oden Institute for Computational Engineering and Sciences, University of Texas at Austin, Austin, USA

Abstract

Optimal experimental design (OED) is a principled framework for maximizing information gained from limited data in inverse problems. Unfortunately, conventional methods for OED are prohibitive when applied to expensive models with high-dimensional parameters, as we target here. We develop a fast and scalable computational framework for goal-oriented OED of large-scale Bayesian linear inverse problems that finds sensor locations to maximize the expected information gain (EIG) for a predicted quantity of interest. By employing low-rank approximations of appropriate operators, an online-offline decomposition, and a new swapping greedy algorithm, we are able to maximize EIG at a cost measured in model solutions that is independent of the problem dimensions. We demonstrate the efficiency, accuracy, and both data- and parameter-dimension independence of the proposed algorithm for a contaminant transport inverse problem with infinite-dimensional parameter field.

1 Introduction

Optimizing the acquisition of data—e.g., what, where, and when to measure, what experiments to run—in order to maximize information gained from the data is a fundamental and ubiquitous problem across all of the natural and social sciences, engineering, medicine, and technology. Just three important examples include optimal observing system design for ocean climate data [37], optimal sensor placement for early warning of tsunami waves [25], and optimal experimental design to accelerate MRI imaging [9]. Bayesian optimal experimental design (BOED)—including formulations as active learning, Bayesian optimization, and sensor placement—provides a probabilistic framework to maximize the expected information gain (EIG) or mutual information (MI) for uncertain parameters or related quantities of interest [15]. However, evaluating the EIG remains prohibitive for large-scale, complex models, due to the need to compute double integrals with respect to both parameter and data distributions. Recently,

This research was partially funded by the National Science Foundation, Division of Mathematical Sciences under award DMS-2012453; the Department of Energy, Office of Science, Office of Advanced Scientific Computing Research, Mathematical Multifaceted Integrated Capability Centers (MMICCS) program under award DE-SC0019303; and the Simons Foundation under award 560651.

advances in efficiently evaluating the EIG and optimizing the design have been achieved using methods based on posterior Laplace approximation-based EIG estimation [36], myopic posterior sampling for adaptive goal-oriented BOED [34], EIG estimation by variational inference for BOED [27], BOED for implicit models by neural EIG estimation [35], and sequential BOED with variable cost structure [45].

Interest has intensified in extending BOED to the case of experiments on, or observations of, complex physical systems, since these can be very expensive (e.g., satellite trajectories, subsurface wells, ocean-bottom acoustic sensors). Such physical systems are typically modeled by partial differential equations (PDEs), which are expensive to solve and often contain infinite-dimensional parameter fields and large numbers of design variable. This presents fundamental challenges to conventional BOED methods, which require prohibitively large numbers of (PDE) model solves. Several different classes of methods have been developed to tackle these computational challenges by exploiting (1) sparsity by polynomial chaos approximation of parameter-to-observation maps [29, 30, 31], (2) intrinsic low dimensionality by low-rank approximation of (prior-preconditioned and data-informed) operators [2, 1, 3, 41, 23, 8], and (3) decomposability by offline (for model-constrained EIG approximation)–online (for design optimization) decomposition [43].

Here, we focus on *goal-oriented* optimal experimental design (GOOED) for large-scale Bayesian inverse problems, in the context of optimal sensor placement. That is, we seek optimal sensor locations that maximize the information gained from the sensors, not about the model parameters, but (of greater practical interest) for a posterior model-predictive goal. In particular, we consider linear parameter-to-observable (PtO) maps governed by expensive models (e.g., PDEs) with high-dimensional uncertain parameters (e.g., infinite-dimensional before discretization). In [8], a gradient-based optimization method is developed to solve the linear GOOED problem to find the optimal sensor locations. However, in each of the possibly very large number of iterations, many model evaluations have to be performed, which makes the algorithm prohibitive if each model evaluation (e.g., solving PDEs) is very expensive.

Contributions. We propose a fast and scalable computational framework for high-dimensional and Bayesian GOOED problems governed by large-scale, expensive-to-solve models. To overcome the curse-of-dimensionality with respect to both parameter and data dimensions, we exploit the intrinsic low-dimensionality of the PtO map and propose and analyze low-rank approximation of appropriate data- and parameter-informed operators and the EIG. These properties are revealed by Jacobians and Hessians of the PtO map, as has been done for model reduction for sampling and deep learning [10, 17, 6, 38], Bayesian inference [13, 14, 16, 21, 22, 18], optimization under uncertainty [4, 20, 19], and BOED [2, 3, 23, 41, 8, 43]. We use a randomized algorithm for the low-rank approximation, which requires only a small and dimension-independent number of large-scale model evaluations. Moreover, we develop an efficient offline-online decomposition scheme to evaluate the *goal-oriented* EIG, where in the offline stage the model-constrained low-rank approximations are performed just once, while in the online stage the design optimization is performed free of model evaluations. Furthermore, for the design optimization we introduce a new swapping greedy algorithm that first constructs an initial set of sensors using leverage scores, and then swaps the chosen sensors with other candidates until certain convergence criteria are met. Finally, we demonstrate the efficiency, accuracy, and dimension independence (with respect to both data and parameters) of the proposed algorithm for a contaminant transport inverse problem with infinite-dimensional parameter field.

We present background on BOED in Section 2, propose our computational framework for GOOED in Section 3, and report results on experiments in Section 4.

2 Background

2.1 Linear Bayesian inverse problem

We consider a general linear model

$$\mathbf{y} = \mathbf{F}\mathbf{m} + \boldsymbol{\epsilon}, \quad (1)$$

where $\mathbf{y} \in \mathbb{R}^{d_y}$ is a d_y -dimensional observational data vector corrupted by additive Gaussian noise $\boldsymbol{\epsilon} \in \mathcal{N}(\mathbf{0}, \boldsymbol{\Gamma}_n)$ with zero mean and covariance $\boldsymbol{\Gamma}_n \in \mathbb{R}^{d_y \times d_y}$, $\mathbf{m} \in \mathbb{R}^{d_m}$ is a d_m -dimensional uncertain parameter vector, and $\mathbf{F} : \mathbb{R}^{d_m} \mapsto \mathbb{R}^{d_y}$ is a linear PtO map. As a specific case, \mathbf{m} is a discretization (e.g., by finite element method) of an infinite-dimensional parameter field in a model described by PDEs, while \mathbf{F} is implicitly given by solving the PDE model. In this case, the parameter dimension is typically very high, $O(10^6 - 10^9)$ for practical applications.

We assume a Gaussian prior $\mathbf{m} \sim \mathcal{N}(\mathbf{m}_{\text{pr}}, \boldsymbol{\Gamma}_{\text{pr}})$ with mean \mathbf{m}_{pr} and covariance $\boldsymbol{\Gamma}_{\text{pr}}$ for the parameter \mathbf{m} with density

$$\pi_{\text{pr}}(\mathbf{m}) \propto \exp\left(-\frac{1}{2}\|\mathbf{m} - \mathbf{m}_{\text{pr}}\|_{\boldsymbol{\Gamma}_{\text{pr}}^{-1}}^2\right), \quad (2)$$

where $\|\mathbf{m} - \mathbf{m}_{\text{pr}}\|_{\boldsymbol{\Gamma}_{\text{pr}}^{-1}}^2 := (\mathbf{m} - \mathbf{m}_{\text{pr}})^T \boldsymbol{\Gamma}_{\text{pr}}^{-1} (\mathbf{m} - \mathbf{m}_{\text{pr}})$. Then by Bayes' rule the posterior density of \mathbf{m} satisfies

$$\pi_{\text{post}}(\mathbf{m}|\mathbf{y}) \propto \pi_{\text{like}}(\mathbf{y}|\mathbf{m})\pi_{\text{pr}}(\mathbf{m}). \quad (3)$$

Here $\pi_{\text{like}}(\mathbf{y}|\mathbf{m})$ is the likelihood function that satisfies

$$\pi_{\text{like}}(\mathbf{y}|\mathbf{m}) \propto \exp(-\Phi(\mathbf{m}, \mathbf{y})) \quad (4)$$

under Gaussian noise $\boldsymbol{\epsilon} \in \mathcal{N}(\mathbf{0}, \boldsymbol{\Gamma}_n)$, where the potential

$$\Phi(\mathbf{m}, \mathbf{y}) := \frac{1}{2}\|\mathbf{F}\mathbf{m} - \mathbf{y}\|_{\boldsymbol{\Gamma}_n^{-1}}^2. \quad (5)$$

Under the assumption of Gaussian prior and Gaussian noise, the posterior of \mathbf{m} is also Gaussian $\mathcal{N}(\mathbf{m}_{\text{map}}, \boldsymbol{\Gamma}_{\text{post}})$ with mean $\mathbf{m}_{\text{post}} = \boldsymbol{\Gamma}_{\text{post}}(\mathbf{F}^* \boldsymbol{\Gamma}_n^{-1} \mathbf{y} + \boldsymbol{\Gamma}_{\text{pr}}^{-1} \mathbf{m}_{\text{pr}})$ and covariance $\boldsymbol{\Gamma}_{\text{post}} = (\mathbf{H}_m + \boldsymbol{\Gamma}_{\text{pr}}^{-1})^{-1}$, where

$$\mathbf{H}_m = \mathbf{F}^* \boldsymbol{\Gamma}_n^{-1} \mathbf{F} \quad (6)$$

is the (data-misfit) Hessian of the potential $\Phi(\mathbf{m}, \mathbf{y})$, and \mathbf{F}^* is the adjoint of \mathbf{F} , e.g., by solving the adjoint PDE model.

2.2 Bayesian optimal experimental design

2.2.1 Expected information gain

The expected information gain (EIG) is defined as the expected (with respect to data) Kullback-Leibler (KL) divergence between the posterior and the prior distributions,

$$\Psi := \mathbb{E}_{\mathbf{y}}[D_{\text{KL}}(\pi_{\text{post}}(\cdot|\mathbf{y})\|\pi_{\text{pr}})], \quad (7)$$

where the KL divergence is defined as

$$D_{\text{KL}}(\pi_{\text{post}}\|\pi_{\text{pr}}) := \int \ln\left(\frac{d\pi_{\text{post}}}{d\pi_{\text{pr}}}\right) d\pi_{\text{post}}. \quad (8)$$

For a Bayesian linear inverse problem as formulated in Section 2.1, the EIG Ψ admits the closed form [1]

$$\Psi = \frac{1}{2} \log \det \left(\mathbf{I}_m + \tilde{\mathbf{H}}_m \right), \quad (9)$$

where \mathbf{I}_m is an identity matrix of size $d_m \times d_m$, and $\tilde{\mathbf{H}}_m := \mathbf{\Gamma}_{\text{pr}}^{\frac{1}{2}} \mathbf{H}_m \mathbf{\Gamma}_{\text{pr}}^{\frac{1}{2}}$ is the *prior-preconditioned Hessian* that includes both data and prior information.

2.2.2 BOED for sensor placement

We consider an optimal sensor placement problem. Assume we have a collection of d candidate sensors $\{s_i\}_{i=1}^d$. We need to choose a much smaller number $r < d$ of sensors (due to a limited budget or physical constraints) at which data are collected. The OED problem seeks to find the best sensor combination from the candidates. We use a Boolean design matrix $W \in \mathcal{W} \subset \mathbb{R}^{r \times d}$ to represent sensor placement such that $W_{ij} = 1$ if the i -th sensor is placed at the j -th candidate location, i.e.,

$$W_{ij} \in \{0, 1\}, \quad \sum_{j=1}^d W_{ij} = 1, \quad \sum_{i=1}^r W_{ij} \in \{0, 1\}. \quad (10)$$

We assume that the observational noise for the d candidate sensors is uncorrelated, with covariance

$$\mathbf{\Gamma}_n^d = \text{diag}(\sigma_1^2, \dots, \sigma_d^2). \quad (11)$$

As a result, for any design W with the covariance for the observation noise ϵ as $\mathbf{\Gamma}_n(W) = W \mathbf{\Gamma}_n^d W^T$, we have

$$\mathbf{\Gamma}_n^{-1}(W) = W(\mathbf{\Gamma}_n^d)^{-1}W^T. \quad (12)$$

Denoting by \mathbf{F}_d the PtO map using all d candidate sensors, we have the design-specific PtO map

$$\mathbf{F}(W) = W \mathbf{F}_d, \quad (13)$$

with its adjoint $\mathbf{F}^* = \mathbf{F}_d^* W^T$. We can now state the OED problem as: find an optimal design $W \in \mathcal{W}$ such that

$$W = \arg \max_{W \in \mathcal{W}} \Psi(W). \quad (14)$$

3 Goal-oriented optimal experimental design

The classical OED problem seeks a design that maximizes the information gain for the parameter vector \mathbf{m} . In this work, we consider a goal-oriented optimal experimental design (GOOED) problem that maximizes the information gain of a predicted *quantity of interest* (QoI) $\rho \in \mathbb{R}^p$, which is assumed to be a linear function of the parameter \mathbf{m} ,

$$\rho = \mathbf{P} \mathbf{m}, \quad (15)$$

where $\mathbf{P} : \mathbb{R}^{d_m} \mapsto \mathbb{R}^{d_\rho}$ is a linear map that typically involves model evaluation (e.g., solving PDEs). Due to linearity, the prior distribution of ρ is Gaussian $\mathcal{N}(\rho_{\text{pr}}, \Sigma_{\text{pr}})$ with mean $\rho_{\text{pr}} = \mathbf{P} \mathbf{m}_{\text{pr}}$ and covariance $\Sigma_{\text{pr}} = \mathbf{P} \mathbf{\Gamma}_{\text{pr}} \mathbf{P}^*$, where \mathbf{P}^* is the adjoint of \mathbf{P} . Moreover, the posterior distribution of ρ is also Gaussian $\mathcal{N}(\rho_{\text{post}}, \Sigma_{\text{post}})$ with mean $\rho_{\text{post}} = \mathbf{P} \mathbf{m}_{\text{post}}$ and covariance $\Sigma_{\text{post}} = \mathbf{P} \mathbf{\Gamma}_{\text{post}} \mathbf{P}^*$.

3.1 Expected information gain for GOOED

To construct an expression for EIG for GOOED, we first introduce Proposition 3.1 [42], which relates the observational data \mathbf{y} and the QoI $\boldsymbol{\rho}$.

Proposition 3.1. *Model (1) and QoI (15) lead to*

$$\mathbf{y} = \mathbf{F}\mathbf{P}_{\dagger}\boldsymbol{\rho} + \boldsymbol{\eta}, \quad (16)$$

where $\mathbf{P}_{\dagger} := \boldsymbol{\Gamma}_{pr}\mathbf{P}^*\boldsymbol{\Sigma}_{pr}^{-1}$, and $\boldsymbol{\eta} \sim \mathcal{N}(\mathbf{0}, \boldsymbol{\Gamma}_{\eta})$ with

$$\boldsymbol{\Gamma}_{\eta} := \boldsymbol{\Gamma}_n + \mathbf{F}(\boldsymbol{\Gamma}_{pr} - \boldsymbol{\Gamma}_{pr}\mathbf{P}^*\boldsymbol{\Sigma}_{pr}^{-1}\mathbf{P}\boldsymbol{\Gamma}_{pr})\mathbf{F}^*, \quad (17)$$

or equivalently $\boldsymbol{\Gamma}_{\eta} = \text{Cov}[\boldsymbol{\epsilon}] + \text{Cov}[\mathbf{F}(\mathbf{I}_m - \mathbf{P}_{\dagger}\mathbf{P})\mathbf{m}]$, with Cov as covariance. Moreover, $\boldsymbol{\rho}$ and $\boldsymbol{\eta}$ are independent.

Thus, the EIG for $\boldsymbol{\rho}$ can be obtained analogously to (9),

$$\Psi^{\rho}(W) = \frac{1}{2} \log \det \left(\mathbf{I}_{\rho} + \tilde{\mathbf{H}}_m^{\rho}(W) \right), \quad (18)$$

where \mathbf{I}_{ρ} is an identity matrix of size $d_{\rho} \times d_{\rho}$, and $\tilde{\mathbf{H}}_m^{\rho}(W) = \boldsymbol{\Sigma}_{pr}^{\frac{1}{2}}\mathbf{H}_m^{\rho}(W)\boldsymbol{\Sigma}_{pr}^{\frac{1}{2}}$, with $\mathbf{H}_m^{\rho}(W)$ given by

$$\mathbf{H}_m^{\rho}(W) = (\mathbf{F}(W)\mathbf{P}_{\dagger})^*\boldsymbol{\Gamma}_{\eta}^{-1}(W)\mathbf{F}(W)\mathbf{P}_{\dagger}. \quad (19)$$

3.2 Offline-online decomposition for EIG Ψ^{ρ}

The EIG $\Psi^{\rho}(W)$ depends on W through $\mathbf{F}(W)$ given in (13), which involves expensive model evaluations (e.g., PDE solutions). Since $\Psi^{\rho}(W)$ must be evaluated repeatedly in the course of maximizing EIG, these repeated model evaluations would be prohibitive. To circumvent this problem, we propose an *offline-online decomposition* scheme, where model-constrained computation of quantities that are independent of W is performed offline a single time, and the online design optimization is free of any model evaluations. The key result permitting this decomposition is given in the following theorem, whose proof is given in Appendix A.

Theorem 3.2. *For each design $W \in \mathcal{W}$, the goal-oriented EIG $\Psi^{\rho}(W)$ given in (18) can be computed as*

$$\Psi^{\rho}(W) = \frac{1}{2} \log \det \left(\mathbf{I}_r + L^T W \mathbf{H}_d^{\rho} W^T L \right), \quad (20)$$

where \mathbf{I}_r is an identity matrix of size $r \times r$, \mathbf{H}_d^{ρ} is given by

$$\mathbf{H}_d^{\rho} := \mathbf{F}_d \boldsymbol{\Gamma}_{pr} \mathbf{P}^* \boldsymbol{\Sigma}_{pr}^{-1} \mathbf{P} \boldsymbol{\Gamma}_{pr} \mathbf{F}_d^*, \quad (21)$$

and L is given by the Cholesky factorization $\boldsymbol{\Gamma}_{\eta}^{-1} = LL^T$.

Note that $\boldsymbol{\Gamma}_{\eta}$ defined in (17) can be equivalently written as

$$\boldsymbol{\Gamma}_{\eta}(W) = W \left(\boldsymbol{\Gamma}_n^d + \mathbf{H}_d - \mathbf{H}_d^{\rho} \right) W^T, \quad (22)$$

where $\mathbf{H}_d := \mathbf{F}_d \boldsymbol{\Gamma}_{pr} \mathbf{F}_d^*$. Hence evaluation of $\Psi^{\rho}(W)$ can be decomposed as follows: (1) construct the model-constrained matrices \mathbf{H}_d and \mathbf{H}_d^{ρ} offline just once; and (2) for each W in the online optimization process, assemble a small $(r \times r)$ matrix $\boldsymbol{\Gamma}_{\eta}(W)$ by (22), compute a Cholesky factorization $\boldsymbol{\Gamma}_{\eta}^{-1} = LL^T$, and assemble $\Psi^{\rho}(W)$ by (20), which are all free of the expensive model evaluations.

Note that $\mathbf{H}_d \in \mathbb{R}^{d \times d}$ and $\mathbf{H}_d^\rho \in \mathbb{R}^{d \times d}$ are large matrices when we have a large number of candidate sensors $d \gg 1$. Moreover, their construction involves expensive model evaluations when the parameters are high-dimensional, $d_m \gg 1$, e.g., by solving PDEs. Therefore, it is computationally not practical to directly compute and store these matrices. Fortunately, the intrinsic ill-posedness of high-dimensional Bayesian inverse problems—data inform only a low-dimensional subspace of parameter space, e.g., [32, 13, 39, 26, 7]—suggests that these matrices are likely low rank or exhibit rapid spectral decay. We exploit this property and construct low-rank approximations of \mathbf{H}_d^ρ and $\mathbf{H}_d - \mathbf{H}_d^\rho$ in the next section.

3.3 Low-rank approximation

Let $\Delta\mathbf{H}_d := \mathbf{H}_d - \mathbf{H}_d^\rho$, where \mathbf{H}_d^ρ and \mathbf{H}_d are given in (21) and (22) and integrate data, parameter, and QoI information. Noting that \mathbf{H}_d^ρ and $\Delta\mathbf{H}_d$ are both symmetric, we compute their low-rank approximation for given tolerances $\epsilon_\zeta, \epsilon_\lambda > 0$ as

$$\hat{\mathbf{H}}_d^\rho = U_k Z_k U_k^T \quad \text{and} \quad \Delta\hat{\mathbf{H}}_d = V_l \Lambda_l V_l^T, \quad (23)$$

where (U_k, Z_k) represent the k dominant eigenpairs of \mathbf{H}_d^ρ with $Z_k = \text{diag}(\zeta_1, \dots, \zeta_k)$ such that

$$\zeta_1 \geq \zeta_2 \geq \dots \geq \zeta_k \geq \epsilon_\zeta \geq \zeta_{k+1} \dots \geq \zeta_d; \quad (24)$$

and (V_l, Λ_l) represent the l dominant eigenpairs of $\Delta\mathbf{H}_d$ with $\Lambda_l = \text{diag}(\lambda_1, \dots, \lambda_l)$ such that

$$\lambda_1 \geq \lambda_2 \geq \dots \geq \lambda_l \geq \epsilon_\lambda \geq \lambda_{l+1} \geq \dots \geq \lambda_d. \quad (25)$$

For the low-rank approximation, we employ a randomized SVD algorithm [28], which requires only $O(k)$ and $O(l)$ model evaluations, respectively. In practice, $k, l \ll d$. More details on the algorithm applied to the example problem in Section 4 can be found in Appendix C.

With $\hat{\Gamma}_\eta(W) := W(\mathbf{\Gamma}_n^d + \Delta\hat{\mathbf{H}}_d)W^T$ as an approximation of $\Gamma_\eta(W)$ in (17), we compute the Cholesky factorization $\hat{\Gamma}_\eta^{-1} = \hat{L}\hat{L}^T$. Then we can define an approximate EIG as

$$\hat{\Psi}^\rho(W) := \frac{1}{2} \log \det \left(\mathbf{I}_r + \hat{L}^T W \hat{\mathbf{H}}_d^\rho W^T \hat{L} \right). \quad (26)$$

The following theorem quantifies the approximation error, whose proof can be found in Appendix B.

Theorem 3.3. *For any design $W \in \mathcal{W}$, the error for the goal-oriented EIG $\Psi^\rho(W)$ in (20) by its approximation $\hat{\Psi}^\rho(W)$ in (26) can be bounded by*

$$\begin{aligned} |\Psi^\rho(W) - \hat{\Psi}^\rho(W)| \leq & \frac{1}{2} \sum_{i=k+1}^d \log(1 + \zeta_i / \sigma_{min}^2) \\ & + \frac{1}{2} \sum_{i=l+1}^k \log(1 + \lambda_i \zeta_1 / \sigma_{min}^4), \end{aligned} \quad (27)$$

where $\sigma_{min}^2 := \min(\sigma_1^2, \dots, \sigma_d^2)$ as defined in (11).

We remark that with rapid decay of the eigenvalues $(\zeta_k)_{k \geq 1}$ of $\hat{\mathbf{H}}_d^\rho$ and $(\lambda_l)_{l \geq 1}$ of $\Delta\hat{\mathbf{H}}_d$, the error bound in (27) becomes very small. Moreover, the decay rates are often independent of the (candidate) data dimension d and the parameter dimension d_m , as demonstrated in Section 4.3. This means that an arbitrarily-accurate EIG approximation can be constructed with a small number, $O(k + l)$, of model solves.

3.4 Swapping greedy optimization

Once the low-rank approximations of \mathbf{H}_d^ρ and $\Delta\mathbf{H}_d$ are constructed per (23), we obtain a fast method for evaluating the approximate EIG in (26), with certified approximation error given by Theorem 3.3. We emphasize that this fast computation does not involve expensive model evaluations (e.g., large-scale PDE solves) for any given design W . We now turn to the (combinatorial) optimization problem of finding the optimal design matrix W ,

$$W = \arg \max_{W \in \mathcal{W}} \hat{\Psi}^\rho(W). \quad (28)$$

We next introduce a swapping greedy algorithm to solve this problem requiring only evaluation of $\hat{\Psi}^\rho(W)$.

In contrast to classical greedy algorithms that sequentially find the optimal sensors one by one (or batch by batch) [11, 33], we extend a swapping greedy algorithm developed for BOED in [43] to solve the GOOED problem. Given a current sensor set, it swaps sensors with the remaining sensors to maximize the approximate EIG $\hat{\Psi}^\rho(W)$ until convergence. To initialize the chosen sensor set, we take advantage of the low-rank approximation $\hat{\mathbf{H}}_d^\rho$ in (23), which contains information from the data (through \mathbf{F}_d), parameter (through $\mathbf{\Gamma}_{\text{pr}}$), and QoI (through \mathbf{P}), as can be seen from (21). In particular, the most informative sensors can be revealed by the rows of U_k with the largest norms, or the leverage scores of \mathbf{H}_d^ρ [12]. More specifically, given a budget of selecting r sensors from d candidate locations, we initialize the candidate set $S^0 = \{s_1, \dots, s_r\}$ such that s_i , $i = 1, \dots, r$, is the row index corresponding to the i -th largest row norm of U_k , i.e.,

$$s_i = \arg \max_{s \in S \setminus S_{i-1}} \|U_k(s, :)\|_2, \quad i = 1, \dots, r, \quad (29)$$

where $U_k(s, :)$ is the s -th row of U_k , $\|\cdot\|_2$ is the Euclidean norm, and the set $S_{i-1} = \{s_1, \dots, s_{i-1}\}$ for $i = 2, 3, \dots$, and $S_0 = \emptyset$. Then at each step of a loop for $t = 1, \dots, r$, we swap a sensor s_t from the current chosen sensor set S^{t-1} with one from the candidate set such that the approximate EIG $\hat{\Psi}^\rho(W)$ evaluated as in (26) can be maximized, i.e., we choose s^* such that

$$s^* = \arg \max_{s \in \{s_t\} \cup (S \setminus S^{t-1})} \hat{\Psi}^\rho(W_s), \quad (30)$$

where W_s is the design matrix corresponding to the sensor choice $S^{t-1} \setminus \{s_t\} \cup \{s\}$. We repeat the loop until a convergence criterion is met, e.g., the chosen S does not change or the difference of the approximate EIG is smaller than a given tolerance. We summarize the swapping algorithm algorithm

in Algorithm 1.

Algorithm 1: A swapping greedy algorithm for GOOED

- 1: **Input:** low-rank approximations (23), a set $S = \{1, \dots, d\}$ of d candidate sensors, a budget of r sensors to be placed.
 - 2: **Output:** the optimal sensor set S^* with r sensors.
 - 3: Initialize $S^* = \{s_1, \dots, s_r\} \subset S$ according to (29).
 - 4: Set $S^0 = \{\emptyset\}$.
 - 5: **while** $S^* \neq S^0$ **do**
 - 6: $S^0 \leftarrow S^*$.
 - 7: **for** $t = 1, \dots, r$ **do**
 - 8: Choose s^* according to (30).
 - 9: Update $S^t \leftarrow (S^{t-1} \setminus \{s_t\}) \cup \{s^*\}$.
 - 10: **end for**
 - 11: Update $S^* \leftarrow S^r$.
 - 12: **end while**
 - 13: **Output:** optimal sensor choice S^* .
-

4 Experiments

In this section, we present results of numerical experiments for GOOED governed by a linear dynamical PDE model with infinite-dimensional parameter field and varying numbers of candidate sensors. This problem features the key challenges of (1) expensive model evaluation and (2) high-dimensional parameters and data. The code is available at <https://github.com/cpempire/GOOED>.

4.1 Model settings

We consider sensor placement for Bayesian inversion of a contaminant source with the goal of maximizing information gain for contaminant concentration on some building surfaces. The transport of the contaminant can be modeled by the time-dependent advection-diffusion equation with homogeneous Neumann boundary condition,

$$\begin{aligned} u_t - k\Delta u + \mathbf{v} \cdot \nabla u &= 0 \text{ in } \mathcal{D} \times (0, T), \\ u(\cdot, 0) &= m \text{ in } \mathcal{D}, \\ k\nabla u \cdot \mathbf{n} &= 0 \text{ on } \partial\mathcal{D} \times (0, T), \end{aligned} \tag{31}$$

where $k = 0.001$ is the diffusion coefficient and $T > 0$ is the final time. The domain $\mathcal{D} \subset \mathbb{R}^2$ is open and bounded with boundary $\partial\mathcal{D}$ depicted in Figure 1. The initial condition m is an infinite-dimensional random parameter field in \mathcal{D} , which is to be inferred. The velocity field $\mathbf{v} \in \mathbb{R}^2$ is obtained as the solution of the steady-state Navier–Stokes equations with Dirichlet boundary condition,

$$\begin{aligned} -\frac{1}{\text{Re}}\Delta \mathbf{v} + \nabla q + \mathbf{v} \cdot \nabla \mathbf{v} &= 0 \text{ in } \mathcal{D}, \\ \nabla \cdot \mathbf{v} &= 0 \text{ in } \mathcal{D}, \\ \mathbf{v} &= \mathbf{g} \text{ on } \partial\mathcal{D}, \end{aligned} \tag{32}$$

where q represents the pressure field and the Reynolds number $\text{Re} = 50$. The Dirichlet boundary data $\mathbf{g} \in \mathbb{R}^2$ are prescribed as $\mathbf{g} = (0, 1)$ on the left wall of the domain, $\mathbf{g} = (0, -1)$ on the right wall, and $\mathbf{g} = (0, 0)$ elsewhere.

We consider a Gaussian prior for the parameter $m \sim \mathcal{N}(m_{\text{pr}}, \mathcal{C}_{\text{pr}})$ with mean m_{pr} and covariance

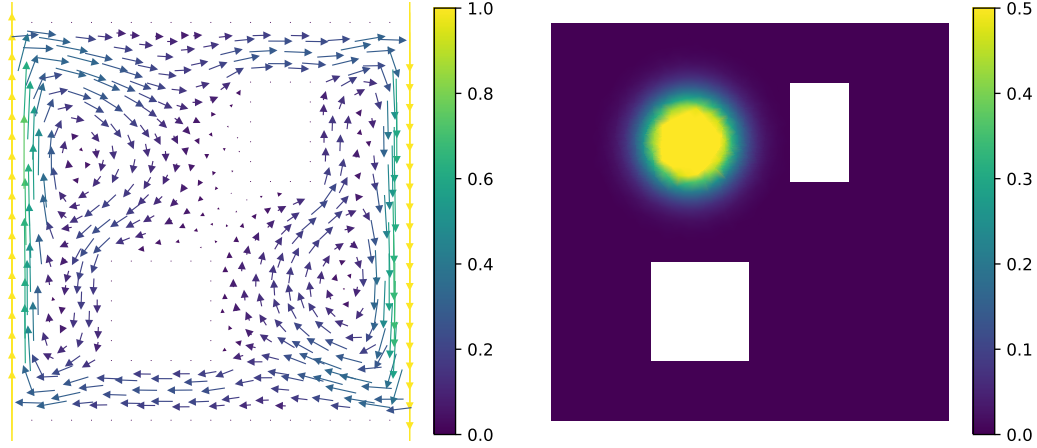


Figure 1: The domain \mathcal{D} is $[0, 1]^2$ with two buildings (rectangles occupying $[0.25, 0.5] \times [0.15, 0.4]$, $[0.6, 0.75] \times [0.6, 0.85]$) removed. Left: velocity field \mathbf{v} . Right: true parameter field m_{true} .

operator $\mathcal{C}_{\text{pr}} = \mathcal{A}^{-2}$, where the elliptic operator $\mathcal{A} = -\gamma\Delta + \delta I$ (with Laplacian Δ and identity I) is equipped with Robin boundary condition $\gamma\nabla m \cdot \mathbf{n} + \beta m$ on $\partial\mathcal{D}$. Here $\gamma, \delta > 0$ control the correlation length and variance of m [24]. In our numerical test, we set $m_{\text{pr}} = 0.25$, $\gamma = 1$, $\delta = 8$. We synthesize a “true” initial condition $m_{\text{true}} = \min(0.5, \exp(-100 \|x - [0.35, 0.7]\|^2))$ as the contaminant source (Figure 1). To solve the PDE model, we use an implicit Euler method for temporal discretization with N_t time steps, and a finite element method for spatial discretization, resulting in a d_m -dimensional discrete parameter $\mathbf{m} \sim \mathcal{N}(\mathbf{m}_{\text{pr}}, \mathbf{\Gamma}_{\text{pr}})$, with $\mathbf{m}_{\text{pr}}, \mathbf{\Gamma}_{\text{pr}}$ denoting finite element discretizations of $m_{\text{pr}}, \mathcal{C}_{\text{pr}}$, respectively.

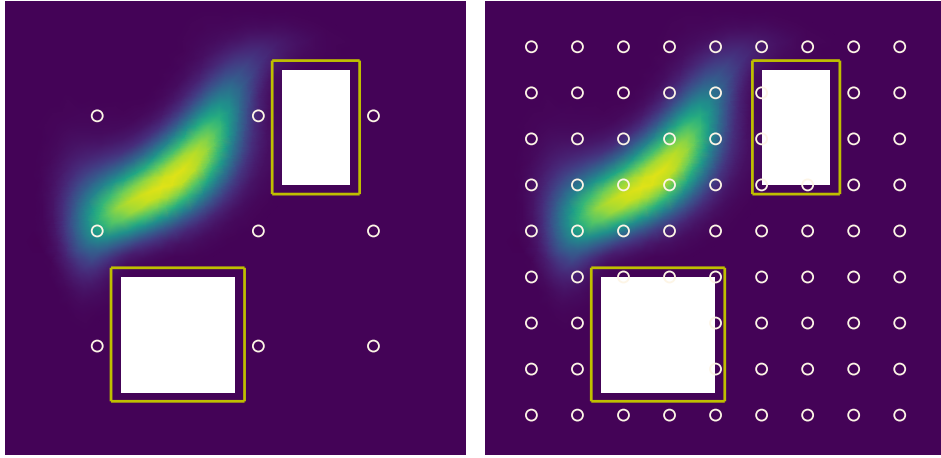


Figure 2: Data of contaminant concentration at time $T = 0.8$, obtained as the solution of (31) at the initial condition shown in Figure 1. The QoI maps $(\mathbf{P}_1, \mathbf{P}_2, \mathbf{P}_3)$ are the averaged solution within the lines along the left, right, and both buildings. Candidate sensor locations are shown in circles (9 left and 75 right).

The solution of the PDE for $d_m = 2023$ and $N_t = 40$ is shown in Figure 2 at the observation time $T = 0.8$. The d candidate sensor locations are also shown in Figure 2, at which we observe the contaminant concentration u . The linear map \mathbf{F} is defined by the predicted data, i.e., the concentrations

at the selected sensors. Finally, we take the QoI as an averaged contaminant concentration at time t_{pred} within a distance $\delta = 0.02$ from the boundaries of either the left, the right, or both buildings, with corresponding QoI maps denoted as $\mathbf{P}_1, \mathbf{P}_2, \mathbf{P}_3$ (see Figure 2).

4.2 Numerical results

We first consider the case of a small number of candidate sensors, for which we can use exhaustive search to find the optimal sensor combination and compare it with the sensors chosen by the standard and swapping greedy algorithms. Specifically, we use a grid of $d = 9$ candidate locations $\{s_i\}_{i=0}^9$ ($x_i \in \{0.2, 0.55, 0.8\} \times \{0.25, 0.5, 0.75\}$) as shown in Figure 2 (left) with the goal of choosing $r = 2, 3, 4, 5, 6, 7, 8$ sensors for the QoI prediction time $t_{\text{pred}} = 1.0$. We compute the matrices \mathbf{H}_d^ρ and $\Delta\mathbf{H}_d$ (of size 9×9) without low-rank approximation since they are small.

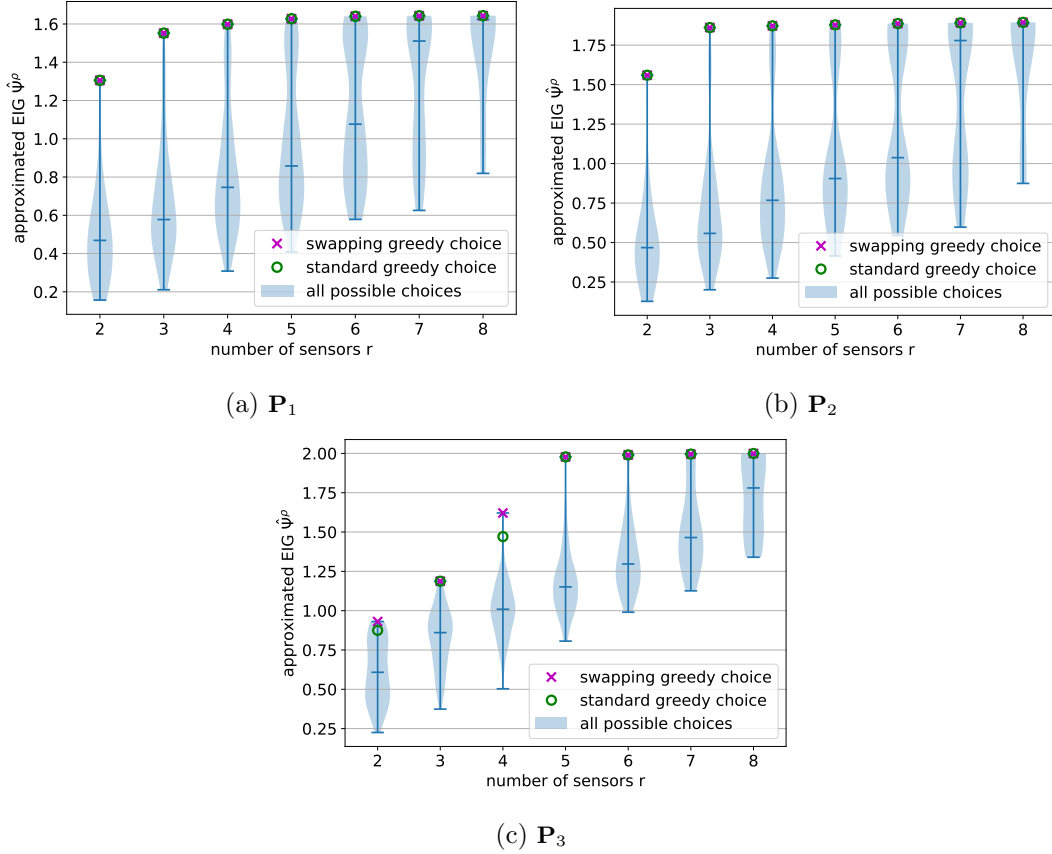


Figure 3: Approximate EIG $\hat{\Psi}^\rho$ at r sensors chosen by the standard and swapping greedy algorithms, and the distribution of $\hat{\Psi}^\rho$ at all possible combinations of 9 candidate sensors. The three plots are for the QoI maps $\mathbf{P}_1, \mathbf{P}_2$, and \mathbf{P}_3 .

We can see from Figure 3 that for QoI maps \mathbf{P}_1 and \mathbf{P}_2 , both greedy algorithms find the optimal design, while for \mathbf{P}_3 with $r = 2, 4$, only swapping greedy finds the optimal design. Moreover, an increase in r leads to diminishing returns, as the gain in information about the QoI from additional sensors saturates. We see that ~ 3 sensors is sufficient for either building, whereas 5 is sufficient for both.

Next we consider the case of the 75 candidate sensors depicted in Figure 2 (right). Exhaustive search across all sensor combinations is not feasible in this case; instead, we compare the best EIG

from 200 random designs with those obtained by the greedy algorithms. We seek the r optimal sensors, $r = 5, 10, 15, 20, 25, 30, 40, 50, 60$, from among the 75 candidates. Results are shown in Figure 4.

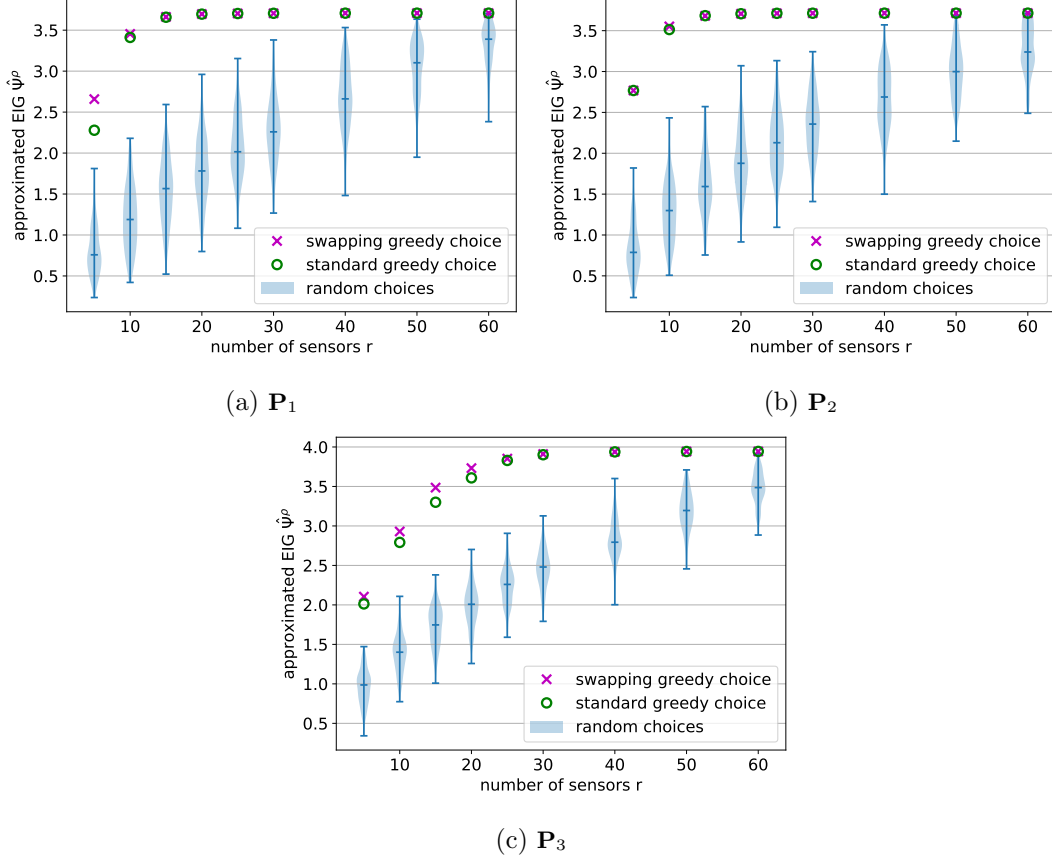


Figure 4: Approximate EIG $\hat{\psi}^\rho$ for r out of 75 sensors, found by the standard and swapping greedy algorithms, compared with the distribution of $\hat{\psi}^\rho$ for 200 randomly-chosen sets from the 75. The three plots are for the QoI maps \mathbf{P}_1 , \mathbf{P}_2 and \mathbf{P}_3 .

We see that both greedy algorithms find designs with larger EIG than all random choices. Moreover, for small r , the swapping greedy algorithm finds better designs than the standard greedy. For large r , both greedy algorithms can find designs with similar EIG. In fact, multiple designs with similar EIG become more likely with larger r .

To demonstrate the reduction of computational cost achieved by the offline-online decomposition, we report the total number of EIG evaluations, the number of swapping loops, and the number of swaps of the swapping greedy algorithm (Algorithm 1) in Table 1 for 75 candidate sensors with different target number of sensors. We see that the number of loops at convergence is mostly 3. We observe in the experiments that most of the swaps take place in the first loop, followed by a smaller number of swaps in the second loop resulting in slight sensor adjustments. There are no swaps in the last loop, which we require as a convergence criterion. As a result of the offline-online decomposition (Theorem 3.2), which relieves the (thousands of) EIG evaluations of expensive PDE solves once the low-rank approximation (23) is built, we achieve over 1000X speedup. This is because the PDE solves overwhelmingly dominate the overall cost, and because the offline decomposition is computed at a cost comparable to one direct EIG evaluation by (18).

Table 1: Number of swapping loops (#LOOPS), swaps (# SWAPS), and EIG evaluations (# EIG EVAL) for different numbers of r selected sensors out of 75 candidates. Results are reported for Algorithm 1 for the goal \mathbf{P}_1 .

r	5	10	15	20	25
#LOOPS	3	3	3	3	3
#SWAPS	41	73	124	164	190
#EIG EVAL	1050	1950	2700	3300	3750
r	30	40	50	60	
#LOOPS	2	3	3	3	
#SWAPS	194	235	199	119	
#EIG EVAL	2700	4200	3750	2700	

Figure 5 illustrates the effect of the goal of maximizing information gain for the QoIs from optimally placed sensors. Specifically, for the parameter-to-QoI maps $\mathbf{P}_1, \mathbf{P}_2, \mathbf{P}_3$ that quantify the average contaminant concentration at time $t_{\text{pred}} = 1$ around left, right, and both blocks, the goal-oriented OED finds the sensors depicted in the first row. For \mathbf{P}_1 at longer prediction times $t_{\text{pred}} = 1, 2, 4, 8$, we see in the bottom row of Figure 5 that the optimal sensors are no longer placed in the immediate vicinity of the building, but instead are increasingly dispersed to better detect the now more diffused field. Finally, the ability of GOOED to reduce the posterior variance in the initial condition field is depicted in Figure 6 for different goals $\mathbf{P}_1, \mathbf{P}_2, \mathbf{P}_3$. Compared to a random design (lower right), the three optimal designs lead to lower variance surrounding regions of interest.

4.3 Scalability w.r.t. parameter and data dimensions

Here we demonstrate the fast decay of the eigenvalues of \mathbf{H}_d^ρ and $\Delta\mathbf{H}_d$ with respect to the parameter and data dimensions, as exploited by the algorithms of Section 3.3. For \mathbf{H}_d^ρ defined in (21), we have $\text{rank}(\mathbf{H}_d^\rho) \leq \min(p, d)$ with QoI dimension p and data dimension d . In practice, the QoI is often an averaged quantity with small p , so the rank of \mathbf{H}_d^ρ is also small. In our tests we have $\text{rank}(\mathbf{H}_d^\rho) = p = 1$. For $\Delta\mathbf{H}_d = \mathbf{H}_d - \mathbf{H}_d^\rho$ with $\mathbf{H}_d = \mathbf{F}_d \mathbf{\Gamma}_{\text{pr}} \mathbf{F}^*$, the spectrum of $\Delta\mathbf{H}_d$ depends on that of \mathbf{H}_d , which typically exhibits fast decay due to ill-posedness of inverse problems. As can be observed in the left plot of Figure 7, the eigenvalues of $\Delta\mathbf{H}_d$ decay very rapidly and independently of the parameter dimension, which implies that the required number of PDE solves is small and independent of the parameter dimension while achieving the same absolute accuracy of the approximate EIG by Theorem 3.3. The right plot in Figure 7 also illustrates rapid decay of eigenvalues, as well as diminishing returns, with increasing number of candidate sensors, suggesting that the number of PDE solves is asymptotically independent of the data dimension for the same relative accuracy of the approximate EIG. These plots suggest that $O(100)$ PDE solves are required to accurately capture the information gained about the parameter field and QoI from the data, regardless of the parameter or sensor dimensions, when using randomized SVD (Algorithm 2).

5 Conclusions

We have developed a fast and scalable computational framework for goal-oriented linear Bayesian optimal experimental design governed by expensive models. Repeated fast evaluation of an (arbitrarily accurate) approximate EIG while avoiding model evaluations is made possible by an offline-online

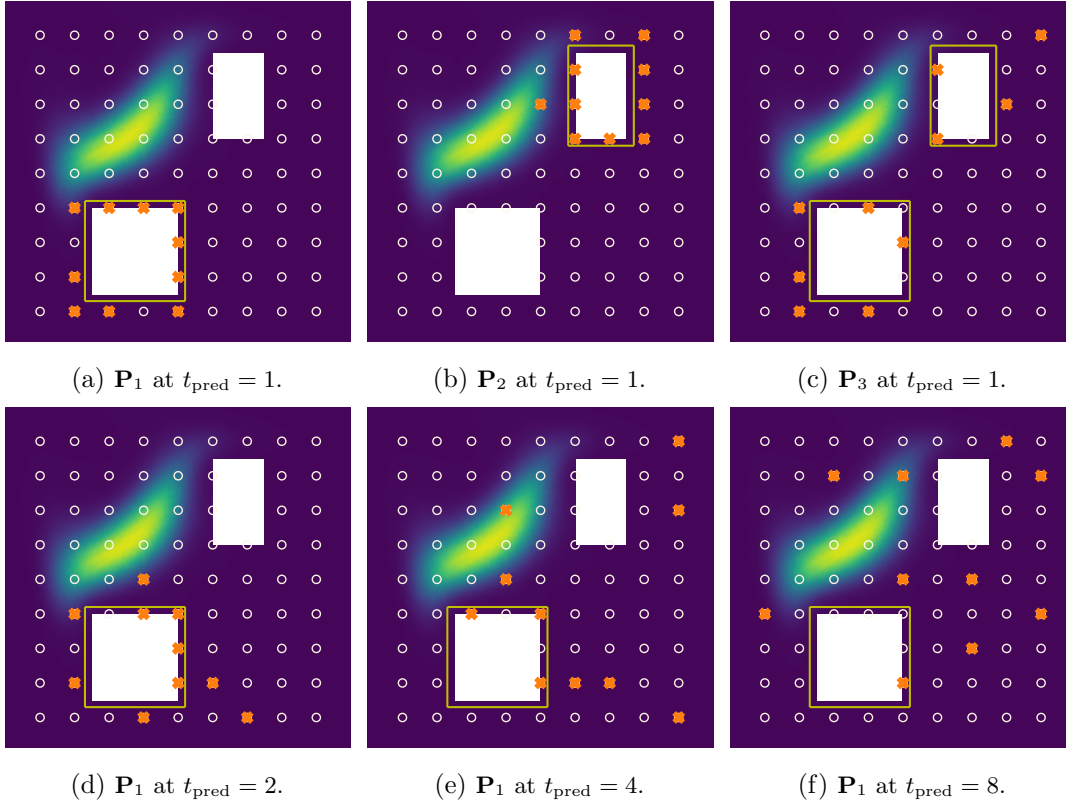
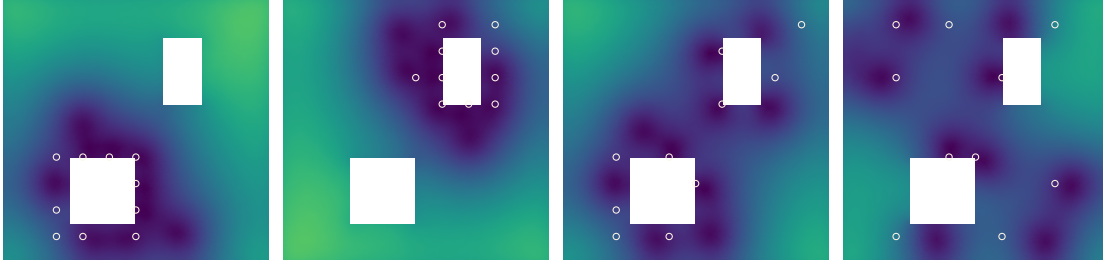


Figure 5: Sensor locations chosen by the swapping greedy algorithm for 10 out of 75 candidates for the parameter-to-QoI maps $\mathbf{P}_1, \mathbf{P}_2, \mathbf{P}_3$ at time $t_{\text{pred}} = 1$ and also \mathbf{P}_1 at time $t_{\text{pred}} = 2, 4, 8$.

decomposition and low-rank approximation of certain operators informed by the parameter, data, and predictive goals of interest. Scalability, as measured by parameter- and data-dimension independence of the number of model evaluations, is achieved by carefully exploiting the GOOED problem’s intrinsic low dimensionality as manifested by the rapid spectral decay of several critical operators. To justify the low-rank approximation of these operators in computing the EIG, we proved an upper bound for the approximation error in terms of the operators’ truncated eigenvalues. Moreover, we proposed a new swapping greedy algorithm that is demonstrated to be more effective than the standard greedy algorithm in our experiments. Numerical experiments with optimal sensor placement for Bayesian inference of the initial condition of an advection–diffusion PDE demonstrated over 1000X speedups (measured in PDE solves). Future work includes extension to nonlinear Bayesian GOOED problems with nonlinear parameter-to-observable maps and nonlinear parameter-to-QoI maps.

References

- [1] Alen Alexanderian, Philip J. Gloor, and Omar Ghattas. On Bayesian A- and D-optimal experimental designs in infinite dimensions. *Bayesian Analysis*, 11(3):671–695, 2016.
- [2] Alen Alexanderian, Noemi Petra, Georg Stadler, and Omar Ghattas. A-optimal design of experiments for infinite-dimensional Bayesian linear inverse problems with regularized ℓ_0 -sparsification.



(a) optimal design for \mathbf{P}_1 (b) optimal design for \mathbf{P}_2 (c) optimal design for \mathbf{P}_3 (d) random design

Figure 6: Pointwise posterior variance of the parameter at optimal designs for goals $\mathbf{P}_1, \mathbf{P}_2, \mathbf{P}_3$, compared to a random design, for 10 sensors. The darker regions represent lower variance.

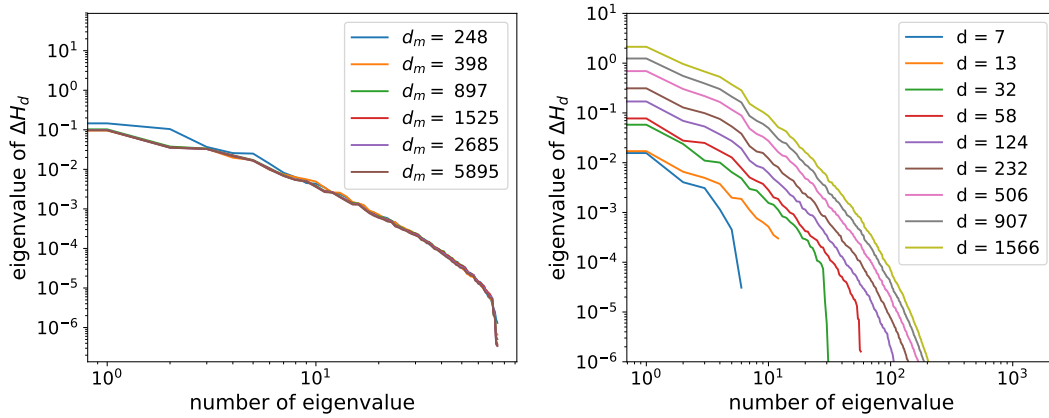


Figure 7: Decay of the eigenvalues of $\Delta \mathbf{H}_d$ with increasing parameter dimension (left) and data (candidate sensor locations) dimension (right).

SIAM Journal on Scientific Computing, 36(5):A2122–A2148, 2014.

- [3] Alen Alexanderian, Noemi Petra, Georg Stadler, and Omar Ghattas. A fast and scalable method for A-optimal design of experiments for infinite-dimensional Bayesian nonlinear inverse problems. *SIAM Journal on Scientific Computing*, 38(1):A243–A272, 2016.
- [4] Alen Alexanderian, Noemi Petra, Georg Stadler, and Omar Ghattas. Mean-variance risk-averse optimal control of systems governed by PDEs with random parameter fields using quadratic approximations. *SIAM/ASA Journal on Uncertainty Quantification*, 5(1):1166–1192, 2017.
- [5] Alen Alexanderian and Arvind K. Saibaba. Efficient D-optimal design of experiments for infinite-dimensional Bayesian linear inverse problems. *SIAM Journal on Scientific Computing*, 40(5):A2956–A2985, 2018.
- [6] Nick Alger, Peng Chen, and Omar Ghattas. Tensor train construction from tensor actions, with application to compression of large high order derivative tensors. *SIAM Journal on Scientific Computing*, 42(5):A3516–A3539, 2020.
- [7] Ilona Ambartsumyan, Wajih Boukaram, Tan Bui-Thanh, Omar Ghattas, David Keyes, Georg Stadler, George Turkiyyah, and Stefano Zampini. Hierarchical matrix approximations of Hessians

- arising in inverse problems governed by PDEs. *SIAM Journal on Scientific Computing*, 42(5):A3397–A3426, 2020.
- [8] Ahmed Attia, Alen Alexanderian, and Arvind K Saibaba. Goal-oriented optimal design of experiments for large-scale bayesian linear inverse problems. *Inverse Problems*, 34(9):095009, 2018.
 - [9] Tim Bakker, Herke van Hoof, and Max Welling. Experimental design for MRI by greedy policy search. *Advances in Neural Information Processing Systems*, 33, 2020.
 - [10] O. Bashir, K. Willcox, O. Ghattas, B. van Bloemen Waanders, and J. Hill. Hessian-based model reduction for large-scale systems with initial condition inputs. *International Journal for Numerical Methods in Engineering*, 73:844–868, 2008.
 - [11] Andrew An Bian, Joachim M Buhmann, Andreas Krause, and Sebastian Tschitschek. Guarantees for greedy maximization of non-submodular functions with applications. In *Proceedings of the 34th International Conference on Machine Learning-Volume 70*, pages 498–507. JMLR. org, 2017.
 - [12] Christos Boutsidis, Michael W. Mahoney, and Petros Drineas. An improved approximation algorithm for the column subset selection problem. *CoRR*, abs/0812.4293, 2008.
 - [13] Tan Bui-Thanh, Carsten Burstedde, Omar Ghattas, James Martin, Georg Stadler, and Lucas C. Wilcox. Extreme-scale UQ for Bayesian inverse problems governed by PDEs. In *SC12: Proceedings of the International Conference for High Performance Computing, Networking, Storage and Analysis*, 2012.
 - [14] Tan Bui-Thanh, Omar Ghattas, James Martin, and Georg Stadler. A computational framework for infinite-dimensional Bayesian inverse problems Part I: The linearized case, with application to global seismic inversion. *SIAM Journal on Scientific Computing*, 35(6):A2494–A2523, 2013.
 - [15] Kathryn Chaloner and Isabella Verdinelli. Bayesian experimental design: A review. *Statistical Science*, 10(3):273–304, 1995.
 - [16] P. Chen, U. Villa, and O. Ghattas. Hessian-based adaptive sparse quadrature for infinite-dimensional Bayesian inverse problems. *Computer Methods in Applied Mechanics and Engineering*, 327:147–172, 2017.
 - [17] Peng Chen and Omar Ghattas. Hessian-based sampling for high-dimensional model reduction. *International Journal for Uncertainty Quantification*, 9(2), 2019.
 - [18] Peng Chen and Omar Ghattas. Projected Stein variational gradient descent. In *Advances in Neural Information Processing Systems*, 2020.
 - [19] Peng Chen, Michael R Haberman, and Omar Ghattas. Optimal design of acoustic metamaterial cloaks under uncertainty. *Journal of Computational Physics*, page 110114, 2021.
 - [20] Peng Chen, Umberto Villa, and Omar Ghattas. Taylor approximation and variance reduction for PDE-constrained optimal control under uncertainty. *Journal of Computational Physics*, 385:163–186, 2019.
 - [21] Peng Chen, Keyi Wu, Joshua Chen, Thomas O’Leary-Roseberry, and Omar Ghattas. Projected Stein variational Newton: A fast and scalable Bayesian inference method in high dimensions. *Advances in Neural Information Processing Systems*, 2019.

- [22] Peng Chen, Keyi Wu, and Omar Ghattas. Bayesian inference of heterogeneous epidemic models: Application to COVID-19 spread accounting for long-term care facilities. *arXiv preprint arXiv:2011.01058*, 2020.
- [23] Benjamin Crestel, Alen Alexanderian, Georg Stadler, and Omar Ghattas. A-optimal encoding weights for nonlinear inverse problems, with application to the Helmholtz inverse problem. *Inverse Problems*, 33(7):074008, 2017.
- [24] Yair Daon and Georg Stadler. Mitigating the influence of boundary conditions on covariance operators derived from elliptic PDEs. *Inverse Problems and Imaging*, 12(5):1083–1102, 2018.
- [25] Angelie R Ferrolino, Jose Ernie C Lope, and Renier G Mendoza. Optimal location of sensors for early detection of tsunami waves. In *International Conference on Computational Science*, pages 562–575. Springer, 2020.
- [26] Pearl H. Flath, Lucas C. Wilcox, Volkan Akçelik, Judy Hill, Bart van Bloemen Waanders, and Omar Ghattas. Fast algorithms for Bayesian uncertainty quantification in large-scale linear inverse problems based on low-rank partial Hessian approximations. *SIAM Journal on Scientific Computing*, 33(1):407–432, 2011.
- [27] Adam Foster, Martin Jankowiak, Elias Bingham, Paul Horsfall, Yee Whye Teh, Thomas Rainforth, and Noah Goodman. Variational Bayesian optimal experimental design. In H. Wallach, H. Larochelle, A. Beygelzimer, F. d'Alché-Buc, E. Fox, and R. Garnett, editors, *Advances in Neural Information Processing Systems*, volume 32, pages 14036–14047. Curran Associates, Inc., 2019.
- [28] Nathan Halko, Per Gunnar Martinsson, and Joel A. Tropp. Finding structure with randomness: Probabilistic algorithms for constructing approximate matrix decompositions. *SIAM Review*, 53(2):217–288, 2011.
- [29] Xun Huan and Youssef M. Marzouk. Simulation-based optimal Bayesian experimental design for nonlinear systems. *Journal of Computational Physics*, 232(1):288–317, 2013.
- [30] Xun Huan and Youssef M. Marzouk. Gradient-based stochastic optimization methods in Bayesian experimental design. *International Journal for Uncertainty Quantification*, 4(6):479–510, 2014.
- [31] Xun Huan and Youssef M Marzouk. Sequential bayesian optimal experimental design via approximate dynamic programming. *arXiv preprint arXiv:1604.08320*, 2016.
- [32] Tobin Isaac, Noemi Petra, Georg Stadler, and Omar Ghattas. Scalable and efficient algorithms for the propagation of uncertainty from data through inference to prediction for large-scale problems, with application to flow of the Antarctic ice sheet. *Journal of Computational Physics*, 296:348–368, September 2015.
- [33] Jayanth Jagalur-Mohan and Youssef Marzouk. Batch greedy maximization of non-submodular functions: Guarantees and applications to experimental design. *arXiv preprint arXiv:2006.04554*, 2020.
- [34] Kirthivasan Kandasamy, Willie Neiswanger, Reed Zhang, Akshay Krishnamurthy, Jeff Schneider, and Barnabas Poczos. Myopic posterior sampling for adaptive goal oriented design of experiments. In *International Conference on Machine Learning*, pages 3222–3232. PMLR, 2019.

- [35] Steven Kleinegesse and Michael U Gutmann. Bayesian experimental design for implicit models by mutual information neural estimation. In *International Conference on Machine Learning*, pages 5316–5326. PMLR, 2020.
- [36] Quan Long, Marco Scavino, Raúl Tempone, and Suojin Wang. Fast estimation of expected information gains for Bayesian experimental designs based on Laplace approximations. *Computer Methods in Applied Mechanics and Engineering*, 259:24–39, 2013.
- [37] Nora Loose and Patrick Heimbach. Leveraging uncertainty quantification to design ocean climate observing systems. *Journal of Advances in Modeling Earth Systems*, pages 1–29, January 2021.
- [38] T. O’Leary-Roseberry, U. Villa, P. Chen, and O. Ghattas. Derivative-informed projected neural networks for high-dimensional parametric maps governed by PDEs. <https://arxiv.org/abs/2011.15110>, 2020.
- [39] Noemi Petra, James Martin, Georg Stadler, and Omar Ghattas. A computational framework for infinite-dimensional Bayesian inverse problems: Part II. Stochastic Newton MCMC with application to ice sheet flow inverse problems. *SIAM Journal on Scientific Computing*, 36(4):A1525–A1555, 2014.
- [40] Constantine Pozrikidis. *An introduction to grids, graphs, and networks*. Oxford University Press, 2014.
- [41] Arvind K Saibaba, Alen Alexanderian, and Ilse CF Ipsen. Randomized matrix-free trace and log-determinant estimators. *Numerische Mathematik*, 137(2):353–395, 2017.
- [42] A. Spantini, T. Cui, K. Willcox, L. Tenorio, and Y. M. Marzouk. Goal-oriented optimal approximations of Bayesian linear inverse problems. *SIAM Journal on Scientific Computing*, 39(5):S167–S196, 2017.
- [43] Keyi Wu, Peng Chen, and Omar Ghattas. A fast and scalable computational framework for large-scale and high-dimensional Bayesian optimal experimental design. *arXiv preprint arXiv:2010.15196*, 2020.
- [44] Man-Chung Yue. A matrix generalization of the hardy-littlewood-pólya rearrangement inequality and its applications. *arXiv preprint arXiv:2006.08144*, 2020.
- [45] Sue Zheng, David Hayden, Jason Pacheco, and John W Fisher III. Sequential Bayesian experimental design with variable cost structure. *Advances in Neural Information Processing Systems*, 33, 2020.

Appendix A: Proof of Theorem 3.2

To start with, we introduce the Weinstein-Aronszajn identity in Proposition .1 which is proven in [40].

Proposition .1. *Let A and B be matrices of size $m \times n$ and $n \times m$ respectively, then*

$$\det(\mathbf{I}_{n \times n} + BA) = \det(\mathbf{I}_{m \times m} + AB). \quad (33)$$

Proof. Considering the design problem defined in Section 2.2.2, for each design with design matrix W , we have

$$\mathbf{F}(W) = W\mathbf{F}_d, \text{ and } \mathbf{\Gamma}_n(W) = W\mathbf{\Gamma}_n^d W^T. \quad (34)$$

We can then reformulate Ψ^ρ with the definition in (18) as

$$\begin{aligned} \Psi^\rho(W) &= \frac{1}{2} \log \det(\mathbf{I} + \tilde{\mathbf{H}}_m^\rho) \\ &= \frac{1}{2} \log \det(\mathbf{I} + \Sigma_{\text{pr}}^{\frac{1}{2}} (W\mathbf{F}_d \mathbf{P}_\dagger)^* \mathbf{\Gamma}_\eta^{-1}(W) (W\mathbf{F}_d \mathbf{P}_\dagger) \Sigma_{\text{pr}}^{\frac{1}{2}}). \end{aligned} \quad (35)$$

where

$$\begin{aligned} \mathbf{\Gamma}_\eta(W) &= \mathbf{\Gamma}_n(W) + \mathbf{F}(W)(\mathbf{\Gamma}_{\text{pr}} - \mathbf{\Gamma}_{\text{pr}} \mathbf{P}^* \Sigma_{\text{pr}}^{-1} \mathbf{P} \mathbf{\Gamma}_{\text{pr}}) \mathbf{F}^*(W) \\ &= W\mathbf{\Gamma}_n^d W^T + W\mathbf{F}_d(\mathbf{\Gamma}_{\text{pr}} - \mathbf{\Gamma}_{\text{pr}} \mathbf{P}^* \Sigma_{\text{pr}}^{-1} \mathbf{P} \mathbf{\Gamma}_{\text{pr}}) \mathbf{F}_d^* W^T \\ &= W(\mathbf{\Gamma}_n^d + \mathbf{F}_d(\mathbf{\Gamma}_{\text{pr}} - \mathbf{\Gamma}_{\text{pr}} \mathbf{P}^* \Sigma_{\text{pr}}^{-1} \mathbf{P} \mathbf{\Gamma}_{\text{pr}}) \mathbf{F}_d^*) W^T \\ &= W(\mathbf{\Gamma}_n^d + \underbrace{\mathbf{F}_d \mathbf{\Gamma}_{\text{pr}} \mathbf{F}_d^*}_{:= \mathbf{H}_d \in \mathbb{R}^{d \times d}} - \underbrace{\mathbf{F}_d \mathbf{\Gamma}_{\text{pr}} \mathbf{P}^* \Sigma_{\text{pr}}^{-1} \mathbf{P} \mathbf{\Gamma}_{\text{pr}} \mathbf{F}_d^*}_{:= \mathbf{H}_d^\rho \in \mathbb{R}^{d \times d}}) W^T \\ &= W(\mathbf{\Gamma}_n^d + \underbrace{\mathbf{H}_d - \mathbf{H}_d^\rho}_{:= \Delta \mathbf{H}_d}) W^T \\ &= W(\mathbf{\Gamma}_n^d + \Delta \mathbf{H}_d) W^T. \end{aligned} \quad (36)$$

To this end, we have

$$\begin{aligned} \Psi(W) &= \frac{1}{2} \log \det \left(\mathbf{I} + \Sigma_{\text{pr}}^{\frac{1}{2}} (W\mathbf{F}_d \mathbf{P}_\dagger)^* \mathbf{\Gamma}_\eta^{-1}(W) (W\mathbf{F}_d \mathbf{P}_\dagger) \Sigma_{\text{pr}}^{\frac{1}{2}} \right) \\ &= \frac{1}{2} \log \det \left(\mathbf{I} + \underbrace{\Sigma_{\text{pr}}^{\frac{1}{2}} (W\mathbf{F}_d \mathbf{P}_\dagger)^*}_A \underbrace{L L^T (W\mathbf{F}_d \mathbf{P}_\dagger) \Sigma_{\text{pr}}^{\frac{1}{2}}}_B \right) \\ &= \frac{1}{2} \log \det \left(\mathbf{I} + \underbrace{L^T (W\mathbf{F}_d \mathbf{P}_\dagger) \Sigma_{\text{pr}}^{\frac{1}{2}}}_B \underbrace{\Sigma_{\text{pr}}^{\frac{1}{2}} (W\mathbf{F}_d \mathbf{P}_\dagger)^*}_A L \right) \\ &= \frac{1}{2} \log \det (\mathbf{I} + L^T (W\mathbf{F}_d \mathbf{P}_\dagger) \Sigma_{\text{pr}} (W\mathbf{F}_d \mathbf{P}_\dagger)^* L) \\ &= \frac{1}{2} \log \det (\mathbf{I} + L^T W \mathbf{F}_d \mathbf{\Gamma}_{\text{pr}} \mathbf{P}^* \Sigma_{\text{pr}}^{-1} \Sigma_{\text{pr}} \Sigma_{\text{pr}}^{-1} \mathbf{P} \mathbf{\Gamma}_{\text{pr}} \mathbf{F}_d^* W^T L) \\ &= \frac{1}{2} \log \det (\mathbf{I} + L^T W \mathbf{F}_d \mathbf{\Gamma}_{\text{pr}} \mathbf{P}^* \Sigma_{\text{pr}}^{-1} \mathbf{P} \mathbf{\Gamma}_{\text{pr}} \mathbf{F}_d^* W^T L) \\ &= \frac{1}{2} \log \det (\mathbf{I} + L^T W \mathbf{H}_d^\rho W^T L), \end{aligned} \quad (37)$$

where we use the Cholesky decomposition $\mathbf{\Gamma}_\eta^{-1} = LL^T$ in the second equality, Proposition .1 in the third, definition of \mathbf{P}_\dagger from (16) in the fifth, and definition of \mathbf{H}_d^ρ from (21) in the last. \square

Appendix B: Proof of Theorem 3.3

To start with, we introduce necessary properties that are proven in [43] for Proposition .2, [5] for Proposition .3 and [44] for Proposition .4.

Proposition .2. *Let A and B be matrices of size $m \times n$ and $n \times m$ respectively, then AB and BA have the same non-zero eigenvalues.*

Proposition .3. *Let $A, B \in \mathbb{C}^{n \times n}$ be Hermitian positive semidefinite with $A \geq B$ (i.e., $A - B$ is Hermitian positive semidefinite), then*

$$0 \leq \log \det(I + A) - \log \det(I + B) \leq \log \det(I + A - B). \quad (38)$$

Proposition .4. *Let $f : \mathbb{R}_+ \rightarrow \mathbb{R}$ be a continuous function that is differentiable on \mathbb{R}_+ (with $x \geq 0$ for $x \in \mathbb{R}_+$). If the function $x \mapsto xf'(x)$ is monotonically increasing on \mathbb{R}_+ . Then for any matrices $A, B \in \mathbb{R}^{n \times m}$, it holds that*

$$\sum_{i=1}^n f(v_i(AB^T)) \leq \sum_{i=1}^n f(v_i(A)v_i(B)) \quad (39)$$

where $v_i(\cdot)$ denotes the singular values of matrices sorted in non-increasing order.

Lemma .5. *Let $A \in \mathbb{R}^{n \times m}$, $B \in \mathbb{R}^{m \times m}$, $A^T A$ and B are Hermitian positive semidefinite, then*

$$\log \det(I + ABA^T) \leq \sum_{i=1}^m \log(1 + v_i(A^T A)v_i(B)). \quad (40)$$

Proof. Since $\log \det(I + ABA^T) = \sum_{i=1}^n \log(1 + v_i(ABA^T)) = \sum_{i=1}^n \log(1 + v_i^2(AB^{1/2}))$, let $f(x) = \log(1 + x^2)$, which satisfies Proposition .4, we have

$$\sum_{i=1}^n \log(1 + v_i^2(AB^{1/2})) \leq \sum_{i=1}^n \log(1 + v_i^2(A)v_i^2(B^{1/2})) = \sum_{i=1}^m \log(1 + v_i(A^T A)v_i(B)). \quad (41)$$

□

To this end, we are at the place to prove Theorem 3.3.

Proof. Denote the eigenvalue decompositions of \mathbf{H}_d^ρ and $\Delta \mathbf{H}_d$ as

$$\mathbf{H}_d^\rho = U_k Z_k U_k^T + U_\perp Z_\perp U_\perp^T, \text{ and } \Delta \mathbf{H}_d = V_l \Lambda_l V_l^T + V_\perp \Lambda_\perp V_\perp^T, \quad (42)$$

where $(Z_k, U_k), (V_l, \Lambda_l)$ represent the dominant eigenpairs, and $(Z_\perp, U_\perp), (V_\perp, \Lambda_\perp)$ represent the remaining eigenpairs. By triangle inequality, we have

$$\begin{aligned} |\Psi^\rho(W) - \hat{\Psi}^\rho(W)| &= \left| \frac{1}{2} \log \det(\mathbf{I}_{r \times r} + L^T W \mathbf{H}_d^\rho W^T L) - \frac{1}{2} \log \det(\mathbf{I}_{r \times r} + \hat{L}^T W \hat{\mathbf{H}}_d^\rho W^T \hat{L}) \right| \\ &\leq \underbrace{\left| \frac{1}{2} \log \det(\mathbf{I}_{r \times r} + L^T W \mathbf{H}_d^\rho W^T L) - \frac{1}{2} \log \det(\mathbf{I}_{r \times r} + L^T W \hat{\mathbf{H}}_d^\rho W^T L) \right|}_{(a)} \\ &\quad + \underbrace{\left| \frac{1}{2} \log \det(\mathbf{I}_{r \times r} + L^T W \hat{\mathbf{H}}_d^\rho W^T L) - \frac{1}{2} \log \det(\mathbf{I}_{r \times r} + \hat{L}^T W \hat{\mathbf{H}}_d^\rho W^T \hat{L}) \right|}_{(b)}. \end{aligned} \quad (43)$$

We first look at (a). By Proposition .3 and note that $(\mathbf{H}_d^\rho - \hat{\mathbf{H}}_d^\rho) = U_\perp Z_\perp U_\perp^T$ is Hermitian positive semidefinite, we have

$$\begin{aligned} (a) &\leq \frac{1}{2} \log \det \left(\mathbf{I}_{r \times r} + L^T W \mathbf{H}_d^\rho W^T L - L^T W \hat{\mathbf{H}}_d^\rho W^T L \right) \\ &= \frac{1}{2} \log \det \left(\mathbf{I}_{r \times r} + L^T W (\mathbf{H}_d^\rho - \hat{\mathbf{H}}_d^\rho) W^T L \right) \\ &= \frac{1}{2} \log \det \left(\mathbf{I}_{r \times r} + L^T W U_\perp Z_\perp U_\perp^T W^T L \right). \end{aligned} \quad (44)$$

Then applying Proposition .1, we have

$$\begin{aligned} (a) &= \frac{1}{2} \log \det \left(\mathbf{I}_{r \times r} + L^T W U_\perp Z_\perp^{1/2} Z_\perp^{1/2} U_\perp^T W^T L \right) \\ &= \frac{1}{2} \log \det \left(\mathbf{I}_{(d-k) \times (d-k)} + Z_\perp^{1/2} U_\perp^T W^T L L^T W U_\perp Z_\perp^{1/2} \right) \\ &= \frac{1}{2} \log \det \left(\mathbf{I}_{(d-k) \times (d-k)} + Z_\perp^{1/2} U_\perp^T W^T (W(\mathbf{\Gamma}_n^d + \Delta \mathbf{H}_d) W^T)^{-1} W U_\perp Z_\perp^{1/2} \right). \end{aligned} \quad (45)$$

Applying Lemme .5, let $A = Z_\perp^{1/2} U_\perp^T W^T$, $B = (W(\mathbf{\Gamma}_n^d + \Delta \mathbf{H}_d) W^T)^{-1}$, we have

$$\begin{aligned} (a) &\leq \frac{1}{2} \sum_i \log(1 + v_i(W U_\perp Z_\perp^{1/2} Z_\perp^{1/2} U_\perp^T W^T) v_i((W(\mathbf{\Gamma}_n^d + \Delta \mathbf{H}_d) W^T)^{-1})) \\ &= \frac{1}{2} \sum_i \log(1 + v_i(W U_\perp Z_\perp U_\perp^T W^T) v_i((W(\mathbf{\Gamma}_n^d + \Delta \mathbf{H}_d) W^T)^{-1})). \end{aligned} \quad (46)$$

By Proposition 3.1, $\Delta \mathbf{H}_d = \text{Cov}[\mathbf{F}_d(I - \mathbf{P}_\dagger \mathbf{P}) \mathbf{m}]$, is a covariance matrix, thus is positive semidefinite. The smallest eigenvalue of $\mathbf{\Gamma}_n^d + \Delta \mathbf{H}_d$ is greater than the smallest eigenvalue of $\mathbf{\Gamma}_n^d$. Hence $v_i(W(\mathbf{\Gamma}_n^d + \Delta \mathbf{H}_d) W^T)) \geq \sigma_{\min}^2$, i.e., $v_i((W(\mathbf{\Gamma}_n^d + \Delta \mathbf{H}_d) W^T)^{-1}) \leq 1/\sigma_{\min}^2$. Note that $v_i(W U_\perp Z_\perp U_\perp^T W^T) \leq v_i(U_\perp Z_\perp U_\perp^T) = \zeta_i$. Thus we have

$$(a) \leq \frac{1}{2} \sum_{i=k+1}^d \log(1 + \zeta_i / \sigma_{\min}^2). \quad (47)$$

Then we turn to second part (b), with Proposition .1 and Proposition .3, we have

$$\begin{aligned} (b) &= \left| -\frac{1}{2} \log \det \left(\mathbf{I}_{r \times r} + L^T W U_k Z_k U_k^T W^T L \right) + \frac{1}{2} \log \det \left(\mathbf{I}_{r \times r} + \hat{L}^T W U_k Z_k U_k^T W^T \hat{L} \right) \right| \\ &= \left| -\frac{1}{2} \log \det \left(\mathbf{I}_{k \times k} + Z_k^{1/2} U_k^T W^T L L^T W U_k Z_k^{1/2} \right) + \frac{1}{2} \log \det \left(\mathbf{I}_{k \times k} + Z_k^{1/2} U_k^T W^T \hat{L} \hat{L}^T W U_k Z_k^{1/2} \right) \right| \\ &\leq \frac{1}{2} \log \det \left(\mathbf{I}_{k \times k} + Z_k^{1/2} U_k^T W^T \hat{L} \hat{L}^T W U_k Z_k^{1/2} - Z_k^{1/2} U_k^T W^T L L^T W U_k Z_k^{1/2} \right) \\ &= \frac{1}{2} \log \det \left(\mathbf{I}_{k \times k} + Z_k^{1/2} U_k^T W^T (\hat{L} \hat{L}^T - L L^T) W U_k Z_k^{1/2} \right) \\ &= \frac{1}{2} \log \det \left(\mathbf{I}_{k \times k} + Z_k^{1/2} U_k^T W^T \underbrace{((W(\mathbf{\Gamma}_n^d + \Delta \hat{\mathbf{H}}_d) W^T)^{-1} - (W(\mathbf{\Gamma}_n^d + \Delta \mathbf{H}_d) W^T)^{-1})}_{(c)} W U_k Z_k^{1/2} \right). \end{aligned} \quad (48)$$

Note that $(A+B)^{-1} = A^{-1} - A^{-1}B(A+B)^{-1}$, let $A = W(\mathbf{\Gamma}_n^d + \Delta \hat{\mathbf{H}}_d) W^T$, $B = W(\Delta \mathbf{H}_d - \Delta \hat{\mathbf{H}}_d) W^T = W V_\perp \Lambda_\perp V_\perp^T W^T$, we have

$$\begin{aligned} (A+B)^{-1} &= (W(\mathbf{\Gamma}_n^d + \Delta \mathbf{H}_d) W^T)^{-1} \\ &= (W(\mathbf{\Gamma}_n^d + \Delta \hat{\mathbf{H}}_d) W^T)^{-1} - (W(\mathbf{\Gamma}_n^d + \Delta \hat{\mathbf{H}}_d) W^T)^{-1} W V_\perp \Lambda_\perp V_\perp^T W^T (W(\mathbf{\Gamma}_n^d + \Delta \mathbf{H}_d) W^T)^{-1} \\ \Rightarrow (c) &= (W(\mathbf{\Gamma}_n^d + \Delta \hat{\mathbf{H}}_d) W^T)^{-1} W V_\perp \Lambda_\perp V_\perp^T W^T (W(\mathbf{\Gamma}_n^d + \Delta \mathbf{H}_d) W^T)^{-1} \end{aligned} \quad (49)$$

Then we can see that

$$\begin{aligned}
(b) &\leq \frac{1}{2} \log \det \left(\mathbf{I}_{k \times k} + Z_k^{1/2} U_k^T W^T (W(\mathbf{\Gamma}_n^d + \Delta \hat{\mathbf{H}}_d) W^T)^{-1} W V_\perp \Lambda_\perp V_\perp^T W^T (W(\mathbf{\Gamma}_n^d + \Delta \mathbf{H}_d) W^T)^{-1} W U_k Z_k^{1/2} \right) \\
&= \frac{1}{2} \log \det \left(\mathbf{I}_{(d-l) \times (d-l)} + \Lambda_\perp^{1/2} V_\perp^T W^T (W(\mathbf{\Gamma}_n^d + \Delta \hat{\mathbf{H}}_d) W^T)^{-1} W U_k Z_k^{1/2} Z_k^{1/2} U_k^T W^T (W(\mathbf{\Gamma}_n^d + \Delta \mathbf{H}_d) W^T)^{-1} W V_\perp \Lambda_\perp^{1/2} \right) \\
&= \frac{1}{2} \log \det \left(\mathbf{I}_{(d-l) \times (d-l)} + \Lambda_\perp^{1/2} V_\perp^T W^T (W(\mathbf{\Gamma}_n^d + \Delta \hat{\mathbf{H}}_d) W^T)^{-1} W U_k Z_k U_k^T W^T (W(\mathbf{\Gamma}_n^d + \Delta \mathbf{H}_d) W^T)^{-1} W V_\perp \Lambda_\perp^{1/2} \right).
\end{aligned} \tag{50}$$

Applying Lemma .5, we have

$$\begin{aligned}
(b) &\leq \frac{1}{2} \sum_i \log(1 + v_i(W V_\perp \Lambda_\perp V_\perp^T W^T) v_i((W(\mathbf{\Gamma}_n^d + \Delta \hat{\mathbf{H}}_d) W^T)^{-1} W U_k Z_k U_k^T W^T (W(\mathbf{\Gamma}_n^d + \Delta \mathbf{H}_d) W^T)^{-1})) \\
&\leq \frac{1}{2} \sum_{i=l+1}^k \log(1 + \lambda_i \zeta_1 / \sigma_{\min}^4),
\end{aligned} \tag{51}$$

where we have used

$$\begin{aligned}
&v_i((W(\mathbf{\Gamma}_n^d + \Delta \hat{\mathbf{H}}_d) W^T)^{-1} W U_k Z_k U_k^T W^T (W(\mathbf{\Gamma}_n^d + \Delta \mathbf{H}_d) W^T)^{-1}) \\
&\leq v_1((W(\mathbf{\Gamma}_n^d + \Delta \hat{\mathbf{H}}_d) W^T)^{-1}) v_1(W U_k Z_k U_k^T W^T) v_1((W(\mathbf{\Gamma}_n^d + \Delta \mathbf{H}_d) W^T)^{-1}) \leq \zeta_1 / \sigma_{\min}^4
\end{aligned} \tag{52}$$

for $i \leq k$ in the last inequality. Note that it vanishes for $i > k$ as Z_k has rank not larger than k . Combining (47) and (51),

$$|\Psi^\rho(W) - \hat{\Psi}^\rho(W)| \leq (a) + (b) \leq \frac{1}{2} \sum_{i=k+1}^d \log(1 + \zeta_i / \sigma_{\min}^2) + \frac{1}{2} \sum_{i=l+1}^k \log(1 + \lambda_i \zeta_1 / \sigma_{\min}^4). \tag{53}$$

□

Appendix C: Low-rank approximation

To compute the low-rank approximations of $\Delta \mathbf{H}_d$ and \mathbf{H}_d^ρ as described in Section 3.3, we present the randomized SVD algorithm for these two quantities. Recall the explicit forms of $\Delta \mathbf{H}_d$ and \mathbf{H}_d^ρ as

$$\mathbf{H}_d^\rho = \mathbf{F}_d \mathbf{\Gamma}_{\text{pr}} \mathbf{P}^* \mathbf{\Sigma}_{\text{pr}}^{-1} \mathbf{P} \mathbf{\Gamma}_{\text{pr}} \mathbf{F}_d^*, \Delta \mathbf{H}_d = \mathbf{F}_d \mathbf{\Gamma}_{\text{pr}} \mathbf{F}_d^* - \mathbf{F}_d \mathbf{\Gamma}_{\text{pr}} \mathbf{P}^* \mathbf{\Sigma}_{\text{pr}}^{-1} \mathbf{P} \mathbf{\Gamma}_{\text{pr}} \mathbf{F}_d^*. \tag{54}$$

Algorithm 2: Randomized SVD to compute \mathbf{H} with low rank k

- 1: Generate i.i.d. Gaussian matrix $\mathbf{\Omega} \in \mathbb{R}^{d \times (k+p)}$ with an oversampling parameter p very small (e.g., $p = 10$).
 - 2: Compute $\mathbf{Y} = \mathbf{H}\mathbf{\Omega}$.
 - 3: Compute the QR factorization $\mathbf{Y} = \mathbf{Q}\mathbf{R}$ satisfying $\mathbf{Q}^T \mathbf{Q} = \mathbf{I}$.
 - 4: Compute $\mathbf{B} = \mathbf{Q}^T \mathbf{H}\mathbf{Q}$.
 - 5: Solve an eigenvalue problem for \mathbf{B} such that $\mathbf{B} = \mathbf{Z}\mathbf{\Sigma}\mathbf{Z}^T$.
 - 6: Form $U_k = \mathbf{Q}\mathbf{Z}[1:k]$ and $\Sigma_k = \mathbf{\Sigma}[1:k, 1:k]$.
-

We see that this is a matrix-free eigensolver. Steps 2 and 4 represent $\Delta \mathbf{H}_d$ action on $O(2(l+p))$ vectors and \mathbf{H}_d^ρ action on $O(2(k+p))$ vectors. In terms of the total actions, it requires $2(2l+k+p)$ forward operator \mathbf{F} and $2(l+k+p)$ of its adjoint \mathbf{F}^* , $2(k+l+p)$ prediction operator \mathbf{P} and its adjoint \mathbf{P}^* .

For the contaminant problem given in Section 4.1, the concentration field $u(x, t)$ is given by

$$\begin{aligned} u_t - k\Delta u + \mathbf{v} \cdot \nabla u &= 0 \text{ in } \mathcal{D} \times (0, T), \\ u(\cdot, 0) &= m \text{ in } \mathcal{D}, \\ k\nabla u \cdot \mathbf{n} &= 0 \text{ on } \partial\mathcal{D} \times (0, T), \end{aligned} \tag{55}$$

we can form the parameter-to-observable map $\mathbf{F}\mathbf{m}$ as the discretized value of $\mathcal{B}u(m)$ where \mathcal{B} is the pointwise observation operator. The adjoint problem is a terminal value problem which can be solved backwards in time by the equation:

$$\begin{aligned} -p_t - \nabla \cdot (p\mathbf{v}) - k\Delta p &= \mathcal{B}^*\mathbf{y} \text{ in } \mathcal{D} \times (0, T), \\ p(\cdot, T) &= 0 \text{ in } \mathcal{D}, \\ (p\mathbf{v} + k\nabla p) \cdot \mathbf{n} &= 0 \text{ on } \partial\mathcal{D} \times (0, T). \end{aligned} \tag{56}$$

Then we can define the adjoint of the parameter-to-observable map $\mathbf{F}^*\mathbf{y}$ as the discretized value of $p(x, 0)$ for any \mathbf{y} .